Mining, Metallurgy & Exploration (2021) 38:269–276
https://doi.org/10.1007/s42461-020-00338-y

ORIGINAL ARTICLE

Potential Application of Iron Oxide Nanoparticles Synthesized by Co-Precipitation Technology as a Coagulant for Water Treatment in Settling Tanks

Naeimeh Shabani[1] · Afshin Javadi[1] · Hoda Jafarizadeh-Malmiri[2] · Hamid Mirzaie[1] · Javid Sadeghi[3]

Received: 24 December 2019 / Accepted: 14 October 2020 / Published online: 26 October 2020

Abstract
Iron oxide nanoparticles (Fe_3O_4 NPs), despite their small size, are stable and have a large surface area that allows for absorption and removal of ions as well as turbidity in a short period of time. Thus, the present study addressed the synthesis and characterization of Fe_3O_4 NPs synthesized using the co-precipitation method and evaluated their effect on the coagulation process in water treatment. The Fe_3O_4 NPs characteristics were evaluated as follows: magnetic properties were measured using a vibrating sample magnetometer (VSM), surface area using Brunauer–Emmett–Teller (BET), crystal phase using X-ray diffraction (XRD), and morphology using field emission scanning electron microscopy (FESEM). In addition, the effects of the synthetic Fe_3O_4 NPs on the turbidity reduction of water in various pH levels were evaluated. The synthesized Fe_3O_4 NPs were without any impurity in the sizes of 22–32 nm, surface area of 99.6 m^2/g, pores' mean diameter size of approximately 10.6 nm, and maximum magnetic saturation of 66.21 emu/gram (emu/g). Using 0.2 g of synthetic Fe_3O_4 NPs with an initial turbidity of 17 NTU and pH of 6 could reduce all water turbidity (100%). Considering the cheap and facile production and separation, as well as the possibility to reuse them and reduce the sludge water content, iron oxide Fe_3O_4 NPs can be effectively used for turbidity reduction in the water treatment process.

Keywords Water treatment · Magnetic iron oxide nanoparticles · Fe_3O_4 NPs · Turbidity

1 Introduction

Nanotechnology is the science of studying materials and phenomena at the nanoscale. Fe_3O_4 NPs are smaller than 100 nm in at least one dimension. Fe_3O_4 NPs have extraordinary properties, compared to their classic counterparts, due to their high surface area to volume ratio [1]. Fe_3O_4 NPs can be fabricated using chemical, physical or a combination of both techniques, such as implantation, attrition, pyrolysis, sonochemical, hydrothermal, and co-precipitation. The co-precipitation technique is a conventional, facile, and environmentally friendly process producing various metal oxide nanoparticles, such as Fe_3O_4 NPs. This process does not produce toxic intermediates or dissolvents, does not need precursor complexes, and is produced at temperatures less than 100 °C. The type and ratio of salts used, process temperature, and pH are some important parameters that control the size and morphology of gained Fe_3O_4 NPs [2, 3]. Magnetic nanoparticles have exclusive properties, such as an extensive spontaneous magnetic field that can react quickly similar to huge paramagnetic atoms when placed in a magnetic field. Fe_3O_4 NPs are used more than other magnetic nanoparticles because they have lower toxicity than their metallic counterparts and have extraordinary paramagnetic behavior [4].

In addition to magnetic characteristics, the Fe_3O_4 NPs have high absorption capacity and may be used as a superabsorbent to absorb various water clouding agents such as natural organic matter (NOM), including hydrophobichumic and fulvic acids, hydrophilic acids, proteins, lipids, hydrocarbons and carbohydrates, and suspended solids. Thus, they can

✉ Afshin Javadi
Javadi@iaut.ac.ir

[1] Department of Food hygiene, Tabriz Branch, Islamic Azad University, Tabriz, Iran

[2] Faculty of Chemical Engineering, Sahand University of Technology, Tabriz, Iran

[3] Department of microbiology, Faculty of Medicine, Tabriz University of Medical Sciences, Tabriz, Iran

be used affectively in water treatment applications. Source waters having high concentrations of NOM have accordingly been treated using metal salts. The actual reason for removal of NOM in production of potable water is to stop disinfection by-products (DBPs) from being produced in the process of disinfection. The major clotting mechanisms involve charge neutralization of colloidal NOM, precipitation as humates or fulvates, and co-precipitation by adsorption on the metal hydroxide. The typical procedure in order to remove NOM in water has been clotting using iron and aluminum salts succeeded by a solid–liquid separation process such as sedimentation or dissolved air flotation [5–8]. Today, water treatment has received considerable attention, especially from economic view points [9, 10]. The practiced full-scale treatment sequence included coagulation, flocculation, clearing turbidity by flotation, disinfection with chlorine dioxide, activated carbon filtration, and post-chlorination. Among the water-treatment processes, coagulation is an important stage that can destabilize small suspended particles of water and convert them into a settable large mass that can be easily removed from the system by filtration or decantation. Generally, the absorbents are good coagulants, especially for removing or decreasing the turbidity of systems. The turbidants have almost negative charges that can be neutralized by absorbents and coagulated and precipitated effectively [11, 12]. Aluminum or iron salts are the most used and conventional absorbents for turbidity removal in water treatment processes. However, the large amount of sludge they produce causes environmental concerns [13]. The best way to improve the removal of NOM is to optimize coagulation conditions concerning pH and coagulant dose. The pH of coagulation is said to be the deciding factor for the removal of NOM. In most studies, the optimum values were between 5.2 and 5.8 for aluminum sulfate and from 4.5 to 5.0 for ferric sulfate. Moreover, optimizing the coagulant dose is important because coagulant over-dosing results in an extra amount of sedimentation. Thus, because the metal coagulant addition leads to a pH reduction, the addition of alkaline chemicals is necessary to maintain the coagulation pH within an effective range. On the other hand, under-dosing normally causes excess residual metal in treated water and can lead to an increase in processed water cloudiness. Moreover, the removal can be improved by a choice of a proper coagulant. The abundantly used coagulant in drinking water production is aluminum sulfate. Ferric salts have become more popular coagulants for many reasons, including health worries regarding the unconfirmed link between aluminum and Alzheimer disease. Ferric salts have also been found to remove NOM more actively at low temperature, especially in cold water (< 3 °C), and low turbidity waters [8]. The development of new coagulants is the probable solution to these problems. Recently, the relevant research in the coagulation flocculation field has converged on new materials as coagulants, such as ferrate salt, polymeric aluminum sulfate, cactus as a natural coagulant, ferromagnetic nanoparticle composited PACls, zirconium coagulant, modified clays, chitosan biopolymer, magnetic seeds together with polyaluminum chloride, and tannin-based coagulant [14–21]. Thus, the nano-absorbents, with lower cost, higher efficiency, and more enviromental compatibility, can be suggested as efficient alternatives for the mentioned salts [11, 22]. Due to the high surface area of nano-absorbents, they have a greater absorption rate and absorption efficiency. The van der Waals and ionic interactions are commonly the prevailing sorption mechanism of nano-absorbents, especially Fe_3O_4 NPs [23, 24].

Therefore, this research was aimed to synthesize modified Fe_3O_4 NPs at high efficiency through a co-precipitation technique in order to absorb ionic contaminants, organic matters, and soil in the coagulation flocculation stage of water treatment. After the coagulation process, the synthesized Fe_3O_4 NPs can be simply collected by a magnetic process and reused and minimum water sludge remains in this process.

2 Materials and Methods

2.1 Materials

Ferrous chloride ($FeCl_2.4H_2O$, 198.83 g/mol) and ferric chloride ($FeCl_3.6H_2O$, 270.30 g/mol) were purchased from Darmstadt, Germany. Sodium hydroxide was obtained from Merck, Germany.

2.2 Synthesis of Fe_3O_4 NPs

The Fe_3O_4 NPs were synthesized from $FeCl_2.4H_2O$ and $FeCl_3.6H_2O$ using the co-precipitation method. To 100 mL of deionized water, 0.1 M $FeCl_2.4H_2O$ and 0.2 M $FeCl_3.6H_2O$ were added and retained using a mechanical laboratory stirrer (Heidolph, PZR 2020, USA) until a homogeneous solution was formed. The solution was covered and placed in a water bath at 60 °C and warmed for 15–20 min. Then 14 mL of 25% sodium hydroxide was added to the solution and the formed black precipitate was centrifuged (BADR, Model 8153, USA) for 15 min at 5000 rpm. The Fe_3O_4 NPs were completely separated after centrifugation from the liquid phase and deposited. The supernatant was discarded and washed several times with deionized water, and the precipitate was dried at 60 °C to get the powder form of iron oxide Fe_3O_4 NPs [25]. The Fe_3O_4 NPs were obtained with a dark brown to black color.

2.3 Characterization

The Fe_3O_4 NPs characteristics were evaluated as follows: magnetic properties were measured using a vibrating sample

magnetometer (VSM, MDKF, Iran), surface area and pore size using Brunauer–Emmett–Teller (BET, BelSorp mini II, Japan), crystal phase using X-ray diffraction (XRD, Siemens D500 X-ray, Germany), and morphology using field emission scanning electron microscopy (FESEM, MIRA3 FEG-SEM, Tescan, Czech).

2.4 Coagulation Experiments

To determine the effectiveness of synthesized Fe_3O_4 NPs in removal of water turbidity, they were applied to water samples that originated from the Zarrineh-roud River (East Azerbaijan, Islamic republic of Iran). For this purpose, the upper limit and lower limit for the three-year average were determined. The turbidity of the Zarineh-roud River for three years is shown in Table 1. The highest turbidity limit was 65 NTU, and the lowest turbidity limit was 17 NTU. Source water was collected at 24–26 °C, pH was 8–8.2, EC was 737–1358 micro-Siemens per centimeter (μs/cm), and turbidity was 17–394.5 NTU.

Various dosages of Fe_3O_4 NPs (0.015–0.25 g) were added to 200 mL of surface water samples. Then the water sample was mixed using a mechanical stirrer at 200 rpm for 2 min and stirring was continued at 40 rpm for 10 min. Then the system was placed on the super magnet (1.2 T, 10 × 2 cm) for 5 min, in order to collect Fe_3O_4 NPs, and 20 mL of the suspension supernatant was transferred to another container in order to measure the turbidity [6]. The turbidity of each sample was measured by a portable turbidity meter (HACH Company, 2100P, USA; Range 0–1000 NTU). The experiment was repeated for pH = 6, 7, and 8. The pH of the suspension was adjusted by adding 0.1 M NaOH or 0.1 M HCl using EC and a pH-meter (WTW, 750 pH/ION/Cond, Germany). The temperature of all the experiments was set at 25 ± 1 °C.

2.5 Statistical Analysis

Analysis of variance (ANOVA) comparison of data and optimization was performed using the Minitab statistical package (Minitab v.17 Inc. PA, USA).

Table 1 Water turbidity of the Zarineh-roud River for three years

Seasons	First year	Second year	Third year
Spring(average)	85.33	77.66	154.9
Summer(average)	24.66	18	154.9
Autumn(average)	58.33	20.66	4.8
Winter(average)	15	4.66	26.2

3 Results and Discussion

3.1 Characterizing Synthesized Fe_3O_4 NPs

3.1.1 X-Ray Diffraction (XRD)

X-ray diffraction pattern was gained using Cu*ka*, the X-ray diffraction intensity was recorded as a function of Bragg's 2θ in the angular range of 5–70°. IR spectra were recorded between 500 and 4000 cm^{-1}. Figure 1 represents the Fe_3O_4 magnetic nanoparticles XRD pattern, the XRD peak 2θ values such as 18.3, 35.5, 43.1, 57.0, and 62.6 correspond to (111), (311), (400), (511), and (440) hkl values, respectively, and the JCPDS-ICDD reference pdf No is 11-614. Comparing the peaks, it is clear that the peaks of the synthesized Fe_3O_4 NPs correspond to the standard sample peaks and the presence of Fe_3O_4 NPs is established. The sharpness of the peaks indicate that the synthesized nanoparticles are crystallite and spherical. The average particle sizes of Fe_3O_4 NPs can be judged using the Debye–Scherrer equation, which gives a relationship between peak broadening in XRD and particle size that is shown by the following equation: $d = k\lambda/(\beta \cdot \cos\theta)$, where d is the particle size of the crystal, k is Sherrer constant (0.9), λ is the X-ray wavelength (0.15406 nm), β is the width of the XRD peak at half-height, and θ is the Bragg diffraction angle. Using the Debye–Scherrer equation, the average crystallite sizes of the magnetic Fe_3O_4 NPs are discovered to be in the range of 16–19 nm. The XRD results show smaller measurement compared with the FESEM results. This can be due to the fact that XRD indicates the crystallite size (crystalline domains) according to the Debye–Scherrer formula, which highlights the limit between crystallographic planes of the particles, and FESEM indicates the particle size as an agglomeration of many crystallites. In this way, our results show a good correlation between the SEM and XRD investigations concerning the particle sizes. Liu et al. [26] have also synthesized Fe_3O_4 NPs through the co-precipitation technique. According to their XRD result, 2θ tops 30.1°, 35.5°, 43.1°, 53.4°, 57.0°, and 62.6°, which are distributed to the (220), (311), (400), (422), (511), and (440) hkl value estimations of magnetite stages.

3.1.2 Field Emission Scanning Electron Microscope (FESEM)

Figure 2 shows the FESEM image of synthesized Fe_3O_4 NPs as adsorbent. As depicted in Fig. 2a, the Fe_3O_4 NPs crystals have a smooth surface. Figure 2b proves the almost spherical morphology of nanoparticles with diameter ranged from 22 to 32 nm. The FESEM image also confirms that the Fe_3O_4 NPs formed are spherical. It is considerable that in practical application nanoparticles with diameters less than 10–20 nm will have a reduced effect, due to their lower physical stability and higher susceptibility to agglomeration. Moreover, very small metallic nanoparticles have lower chemical stability and can

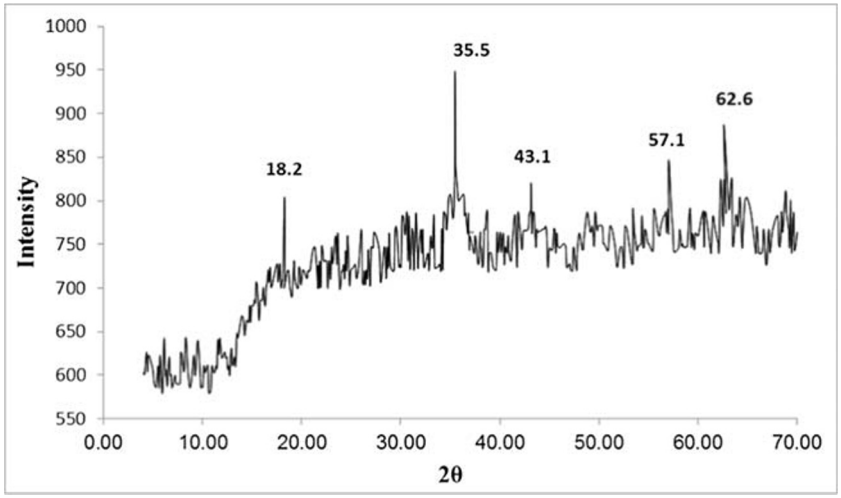

Fig. 1 The XRD pattern of the synthesized Fe_3O_4 NPs

be rapidly oxidized in the presence of oxygen. Previous studies also showed that the approximately 30 nm magnetic Fe_3O_4 NPs have more desired characteristics, such as more electron conductivity and enhanced absorption capability, especially for enzyme immobilization uses, compared to smaller ones [27].

3.1.3 Brunauer–Emmett–Teller (BET) Surface Area Analysis

The pore size, as well as volume and regional distribution can be achieved using BET analysis of mesoporous or macroporous materials. In general, a smaller pore diameter leads to the synthesized particle specific surface area [28]. Figure 3 shows the BET surface area and total pore volume of synthesized Fe_3O_4 NPs. It can be concluded that surface area and total pore volume of gained Fe_3O_4 NPs are 99. 6 m^2 g^{-1} and 22.88 cm^3 g^{-1}, respectively, which were obtained using nitrogen as an adsorptive agent, at an adsorption temperature of 77 K and activation time of 180 min. It should be noted that when Po/P is in the range of 0.3–0.05 multilayer adsorption does not occur in most cases and the adsorption data show good agreement with the BET eq. [29]. Some isotherms have a hysteresis curve, which indicates the presence of mesopores in the material, and can provide information on the geometry of the pores [30]. As can be seen in Fig. 4, the adsorption/desorption isotherm is type IV, and thus the porosity of the synthesized samples is thin and capillary. Consequently, the adsorption rate for Fe_3O_4 NPs is significantly higher with concentrated adsorbed material on the absorbent surfaces. The hysteresis isotherm showed that the diagram of the porosity is cylindrical and the relationship between the sample surface and the adsorbent is relatively

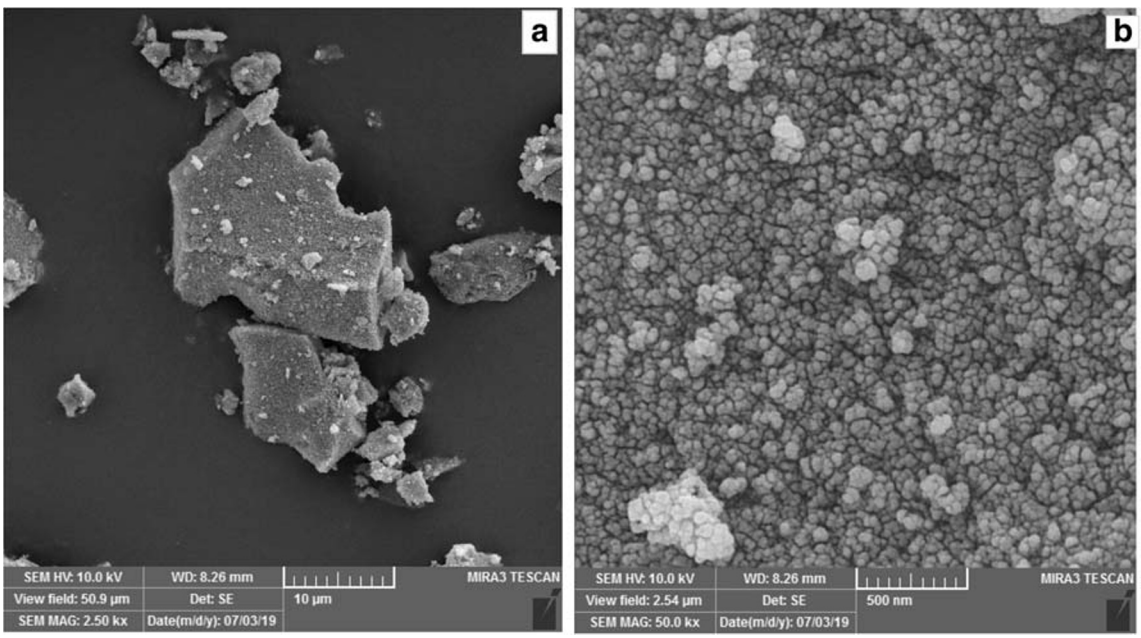

Fig. 2 **a & b** The FESEM images of the synthesized Fe_3O_4 NPs

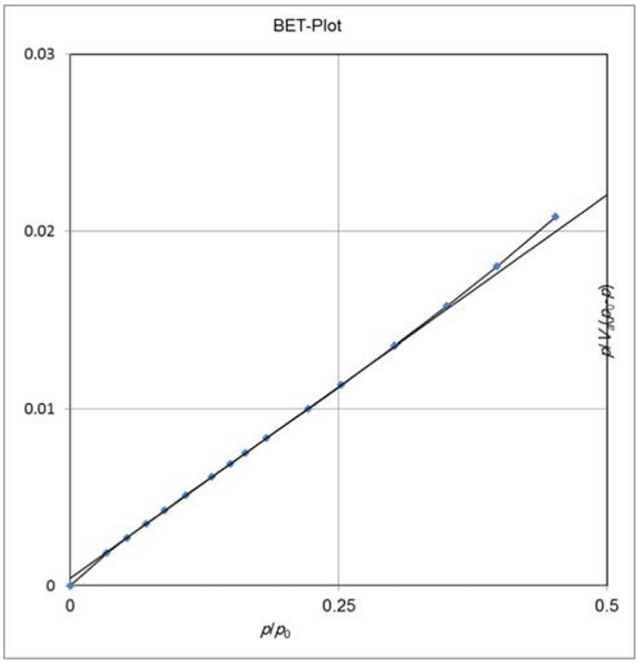

Fig. 3 The BET plot of the synthesized Fe_3O_4 NPs

strong. The mean pore diameter is 10.6 nm and according to the IUPAC classification, the porosity is categorized in the mesopores group. The Barrett, Joyner, and Halenda (BJH) method is used to calculate the diameter of the pores and the regional distribution of the pores. In general, the smaller the pore diameter, the greater the specific surface area of the particles [28]. Figure 5 indicated that the distribution of porosity was homogenous and the diameter peak was 10.7 nm.

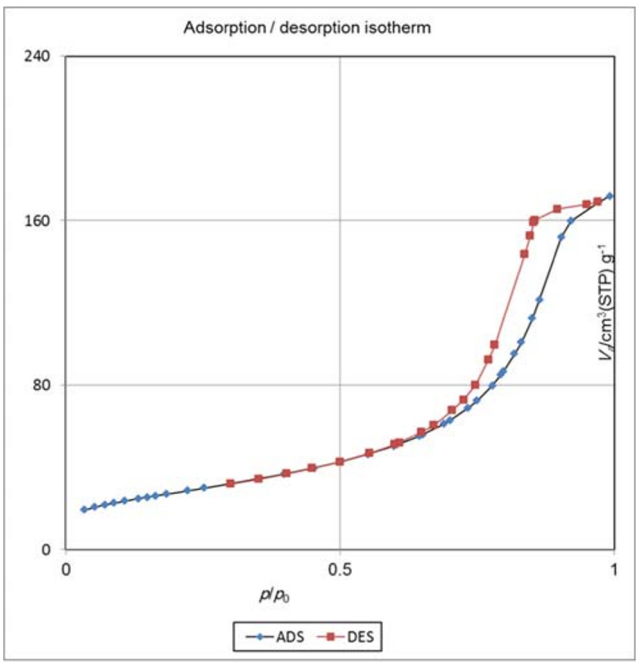

Fig. 4 Adsorption/desorption isotherm of the synthesized Fe_3O_4 NPs

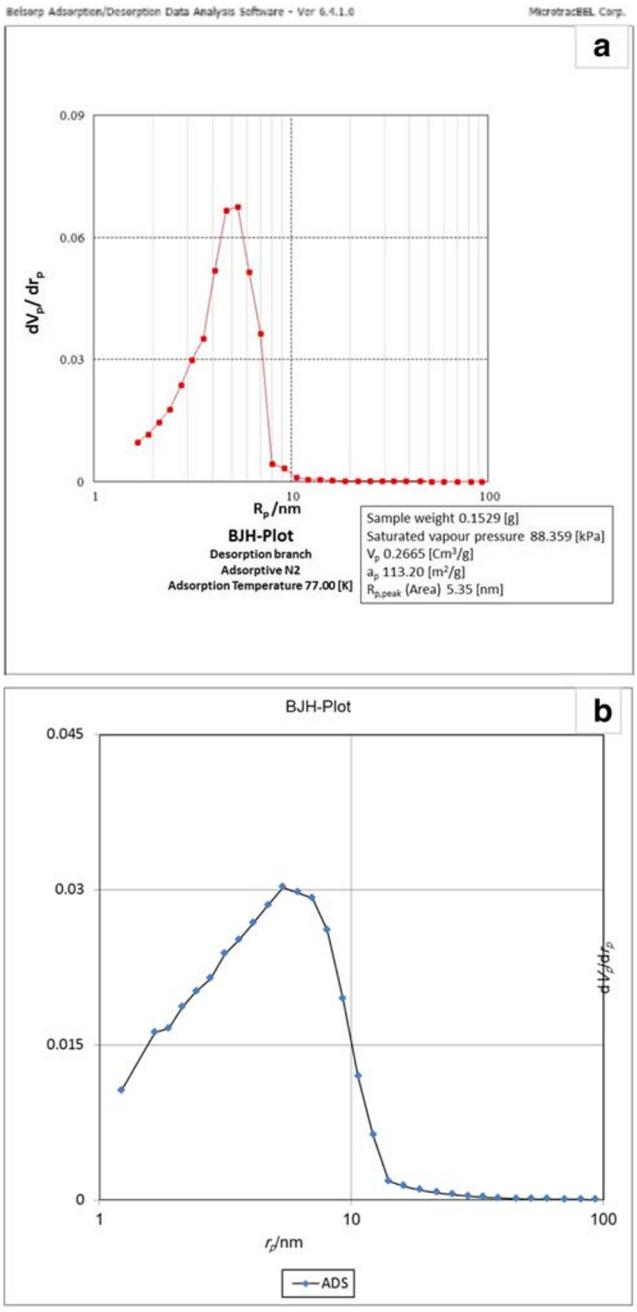

Fig. 5 **a & b** BJH plot of the synthesized Fe_3O_4 NPs

3.1.4 Vibrating Sample Magnetometer (VSM)

In most materials, the spin moments are small and aligned randomly causing para magnetism. In some materials, specifically transition metals such as iron, the spin moments are large and aligned in parallel or ferro magnetically. This causes a net spontaneous magnetic moment in the material [31, 32]. Figure 6 for Fe_3O_4 NPs shows a phenomenal paramagnetic behavior without any obstruction or inclination. The range of the applied field with an intensity of 10,000 Oe, for the

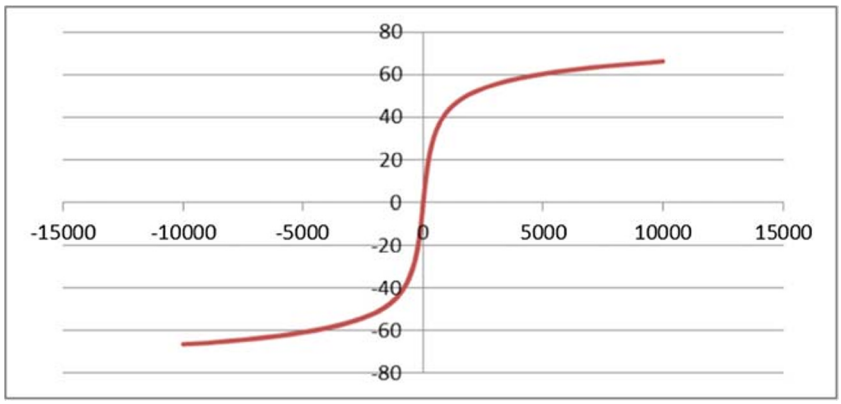

Fig. 6 The VSM of the synthesized Fe_3O_4 NPs

Table 2 Results of ANOVA (F-value and *p*-value)

Source	F-value	*p*-value
Fe_2O_3 NP (g)	17.98	0.00
NTU	18.68	0.00
pH	0.46	0.63

maximum magnetic saturation is 66.21 emu/g. A hysteresis loop with magnetization of this value demonstrates that it has a super paramagnetic nature [33].

3.2 Evaluation of the Coagulation Ability of Fe_3O_4 NPs

The effect of nanoparticle concentration and initial turbidity and pH was analyzed using the generalized linear model (GLM). The analysis of variance in evaluation of the effects of Fe_3O_4 NPs, initial turbidity, and pH on their turbidity reduction ability are depicted in Table 2. As can be seen, the concentration of nanoparticles and turbidity has significant ($p < 0.05$) effects. Although according to a previous study, with an extensive range, pH is the main factor affecting adsorption processes [6], pH was not shown to influence the adsorption of nanoparticles significantly (as indicated by the obtained *p*-value). This could be due to the smaller pH range (pH 6–8) examined in this study. Thus, under the examined pH ranges, the interaction of nanoparticles and H^+ ions could not alter the nanoparticles' electrostatic forces, and consequently, their adsorption capacity.

As shown in Fig. 7, by increasing the quantity of nanoparticles, the amount of turbidity decreases, and by reducing turbidity, the efficiency of absorption was improved. This result is very proficient for purifying low turbidity water. In low turbidity water, the number of impure particles is small and the distribution is relatively uniform. Colloidal particles have small negative potential and strong inter-particle rejection.

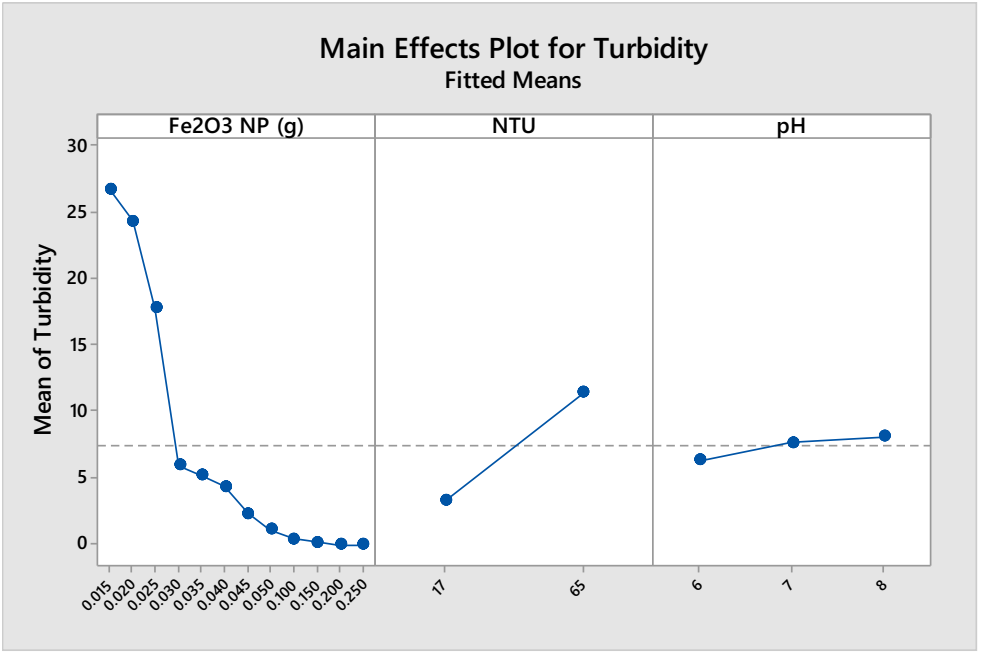

Fig. 7 The effect of nanoparticle concentration and initial turbidity and pH

Accordingly, colloids are difficult to remove and the aggregation effect is poor. Thus, the colloids are difficult to coagulate when an electrolyte or salt is used as coagulant [34]. The turbidity removal ability of Fe_3O_4 NPs is shown in Fig. 8, the turbidity removal efficiency of Fe_3O_4 NPs can be increased effectively by increasing the nanoparticles' dosage. For instance, at a 0.015 g dosage of Fe_3O_4 NPs, the turbidity was reduced by approximately half and by increasing the Fe_3O_4 NPs dosage to 0.035 g, turbidity reached below 10 NTU. For instance, using 0.15 g of Fe_3O_4 NPs approximately 96.15% and 88.82% turbidity can be removed for primary water turbidity of 65 and 17 NTU, respectively. The single optimization results (Fig. 8) indicate that the highest turbidity reduction would occur using 0.2 g of Fe_3O_4 NPs, primary turbidity of 17, and pH of 6. The results of this study are almost compatible with the results of Hatamie et al. [6]. They could remove 95.8% and 86% turbidities of samples with an initial water turbidity of 60 and 24 NTU, respectively, using 0.15 g of 30–50 nm Fe_3O_4 NPs. In other research, 94% of turbidities were removed from the water with an initial turbidity of 80 NTU, using 0.32 g of graphene oxide based nano-absorbents with 10 min contact time [35]. Thus, the Fe_3O_4 NPs are more efficient than graphene oxide based nano-absorbents with similar contact time. Fe_3O_4 NPs can also remove water turbidity in smaller dosages. Fe_3O_4 NPs showed a turbidity removal tendency at neutral pHs, and consequently, they can treat greater amounts of water without any pH regulations. Thus, Fe_3O_4 NPs are appropriate for elimination of several types of ionic and organic contaminants and turbidants from water in a very short period of time [36, 23].

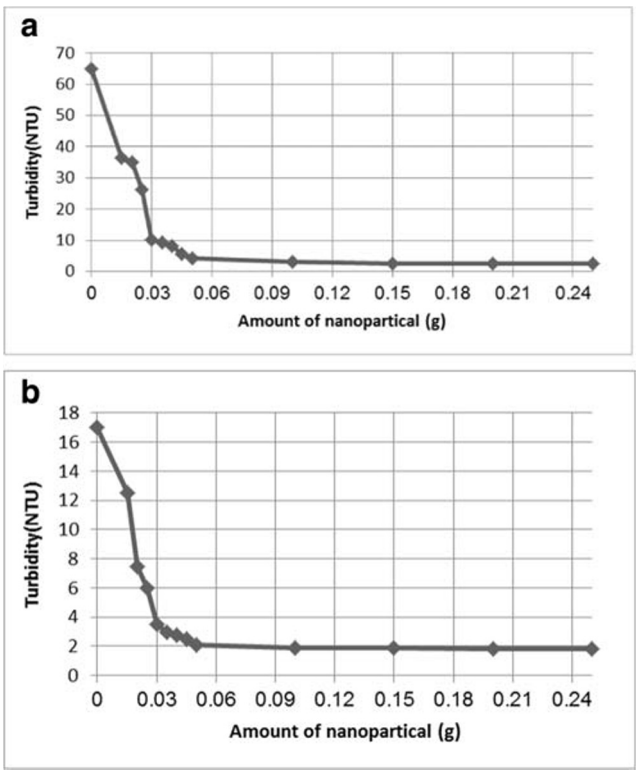

Fig. 8 The effect of the Fe_3O_4 NPs dosage on turbidity removal of 200 mL water with an initial turbidity of (**a**) 65 NTU and (**b**) 17 NTU

4 Conclusions

Fe_3O_4 NPs with high stability were successfully synthesized using a simple co-precipitation method in 23–32 nm mean sizes, in order to absorb and remove the water turbidants and clarify water resources perfectly. The characteristics of the obtained nanoparticles were then evaluated in terms of VSM, BET, XRD, and FESEM to measure magnetic properties, surface area, crystal phase, and morphology, respectively. The synthesized Fe_3O_4 NPs were without any impurity in the sizes of 22–32 nm, surface area of 99.6 m^2/g, pores' mean diameter size of approximately 10.6 nm, and maximum magnetic saturation of 66.21 emu/g. The effects of the synthetic Fe_3O_4 NPs, initial NTU, and pH were then evaluated on turbidity reduction of gained nanoparticles. Using 0.2 g of synthetic Fe_3O_4 NPs with an initial turbidity of 17 NTU and pH of 6 could reduce all water turbidity (100%). Thus, it seems that using Fe_3O_4 NPs as an absorbent in the water treatment process can be an efficient and economical alternative due to their cheap raw materials, facile synthesizing and recovering processes, as well as the ability to reuse them several times.

Acknowledgements This research did not receive any specific grant from funding agencies in the public, commercial, or not-for-profit sectors.

Compliance with ethical standards

Conflict of Interest On behalf of all authors, the corresponding author states that there is no conflict of interest.

References

1. Qu X, Alvarez PJ, Li Q (2013) Applications of nanotechnology in water and wastewater treatment. Water Res 47(12):3931–3946. https://doi.org/10.1016/j.watres.2012.09.058
2. Petcharoen K, Sirivat A (2012) Synthesis and characterization of magnetite nanoparticles via the chemical co-precipitation method. Mater Sci Eng B, Solid-State Mat Adv Technol 177(5):421–427. https://doi.org/10.1016/j.mseb.2012.01.003
3. Aliramaji S, Zamanian A, Sohrabijam Z (2015) Characterization and synthesis of magnetite nanoparticles by innovative Sonochemical method. Procedia Mater Sci 11:265–269. https://doi.org/10.1016/j.mspro.2015.11.022
4. Gutierrez AM, Dziubla TD, Hilt JZ (2017) Recent advances on iron oxide magnetic nanoparticles as sorbents of organic pollutants in water and wastewater treatment. Rev Environ Health 32(1-2):111–117. https://doi.org/10.1515/reveh-2016-0063
5. Buß DH (1992) Iron oxides in the laboratory. Preparation and characterization. Von U. Schwertmann und R. M. Cornell. VCH Verlagsgesellschaft, Weinheim/VCH publishers, New York, 1991. XIV, 137 S. geb. DM 118.00.– ISBN 3-527-26991-6/0-

89573-858-9. Angew Chem 104(11):1569–1569. https://doi.org/10.1002/ange.19921041155
6. Hatamie A, Parham H, Zargar B, Heidari Z (2016) Evaluating magnetic nano-ferrofluid as a novel coagulant for surface water treatment. J Mol Liq 219:694–702. https://doi.org/10.1016/j.molliq.2016.04.020
7. Parsons SA, Jefferson B (2008) Processes for enhanced NOM removal: beyond Fe and Al coagulation. Water Sci Technol: Water Supply—WSTWS 8(6):709–716
8. Matilainen A, Lindqvist N, Tuhkanen T (2005) Comparion of the effiency of aluminium AND ferric sulphate in the removal of natural organic matter during drinking water treatment process. Environ Technol 26:867–875
9. Ali I, Asim M, Khan TA (2012) Low cost adsorbents for the removal of organic pollutants from wastewater. J Environ Manag 113:170–183. https://doi.org/10.1016/j.jenvman.2012.08.028
10. Ali I, Gupta VK (2006) Advances in water treatment by adsorption technology. Nat Protoc 1(6):2661–2667. https://doi.org/10.1038/nprot.2006.370
11. Huang X, Sun S, Gao B, Yue Q, Wang Y, Li Q (2015) Coagulation behavior and floc properties of compound bioflocculant-polyaluminum chloride dual-coagulants and polymeric aluminum in low temperature surface water treatment. J Environ Sci (China) 30:215–222. https://doi.org/10.1016/j.jes.2014.07.033
12. Fatombi JK, Lartiges B, Aminou T, Barres O, Caillet C (2013) A natural coagulant protein from copra (*Cocos nucifera*): Isolation, characterization, and potential for water purification. Sep Purif Technol 116:35–40
13. Jarvis P, Sharp E, Pidou M, Molinder R, Parsons SA, Jefferson B (2012) Comparison of coagulation performance and floc properties using a novel zirconium coagulant against traditional ferric and alum coagulants. Water Res 46(13):4179–4187. https://doi.org/10.1016/j.watres.2012.04.043
14. Jiang JQ, Lloyd B (2002) Water res. Progress in the development and use of ferrate (VI) salt as an oxidant and coagulant for water and wastewater treatment. Water Res 36:1397–1408
15. Zhang X, Hu J, Spanjers H, van Lier JB (2014) Performance of inorganic coagulants in treatment of backwash waters from a brackish aquaculture recirculation system and digestibility of salty sludge. Aquac Eng 61:9–16
16. Zhang J, Zhang F, Luo Y, ng H (2006) A preliminary study on Cactus as coagulant in water treatment. Process Biochem 41(3):730–733. https://doi.org/10.1016/j.procbio.2005.08.016
17. Zhang M, Xiao F, Xu XZ, Wang DS (2012) Novel ferromagnetic nanoparticle composited PACls and their coagulation characteristics. Water Res 46:127–135. https://doi.org/10.1016/j.watres.2011.10.025
18. Jiang JQ, Zeng Z, Pearce P (2004) Pearce, preparation and use of modified clay coagulants for wastewater treatment. Water Air Soil Pollut 158:53–65. https://doi.org/10.1023/B:WATE.0000044833.75579.8b
19. Cheng WP, Chi FH, Yu RF, Lee YC (2005) Using chitosan as a coagulant in recovery of organic matters from the mash and Lauter wastewater of brewery. J Polym Environ 13:383–388
20. Wana TJ, Shen SM, Siao SH, Huang CF, Cheng CY (2011) Using magnetic seeds to improve the aggregation and precipitation of nanoparticles from backside grinding wastewater. Water Res 45:6301–6307. https://doi.org/10.1016/j.watres.2011.08.067
21. Beltran-Heredia J, Sanchez-Martin J, Davila-Acedo MA (2011) Optimization of the synthesis of a new coagulant from a tannin extract. J Hazard Mater 186:1704–1712. https://doi.org/10.1016/j.jhazmat.2010.12.075
22. Nassar NN (2010) Rapid removal and recovery of Pb(II) from wastewater by magnetic nanoadsorbents. J Hazard Mater 184(1-3):538–546. https://doi.org/10.1016/j.jhazmat.2010.08.069
23. Sabzoi N, Siddiqui MTH, Mujawar M, Baloch H, Abdullah E, Mazari S, Griffin G, Srinivasan M, Tanksale A (2018) Iron oxide nanomaterials for the removal of heavy metals and dyes from wastewater. https://doi.org/10.1016/B978-0-12-813926-4.00023-9
24. Nassar NN (2012) Iron oxide nanoadsorbents for removal of various pollutants from wastewater. Appl Adsorbents Water Pollut Control 135:81–118
25. Bellova A, Bystrenova E, Koneracka M, Kopcansky P, Valle F, Tomasovicova N, Timko M, Bagelova J, Biscarini F, Gazova Z (2010) Effect of $Fe_{(3)}O_{(4)}$ magnetic nanoparticles on lysozyme amyloid aggregation. Nanotechnology 21(6):065103. https://doi.org/10.1088/0957-4484/21/6/065103
26. Liu Y, Li X, Bao S, Lu Z, Li Q et al (2013) Plastic protein microarray toinvestigate the molecular pathways of magnetic nanoparticle-induced nano toxicity. Nanotechn 24:175501
27. Lu AH, Salabas EL, Schuth F (2007) Magnetic nanoparticles: synthesis, protection, functionalization, and application. Angewandte Chemie (International ed in English) 46(8):1222–1244. https://doi.org/10.1002/anie.200602866
28. Semsarzadeh MA, Fardi M (2014) SPB_1 and $SPB_{1,2}$: synthesis and determination of the microstructure and physical properties. Iranian J Polymer Sci Technol 27(2):161–171
29. Legras A, Kondor A, Heitzmann MT, Truss RW (2015) Inverse gas chromatography for natural fibre characterisation: identification of the critical parameters to determine the Brunauer-Emmett-Teller specific surface area. J Chromatogr A 1425:273–279. https://doi.org/10.1016/j.chroma.2015.11.033
30. Brunauer S, Emmett PH, Teller E (2006) Seminar and practical training short course, BET surface area analyzer, Rice University, Houston. J Am Chem Soc pp 18–19
31. Kirupakar BR, Vishwanath BA, Padma Sree M (2016) Vibrating sample magnetometer and its application in characterisation of magnetic property of the anti cancer drug magnetic microspheres. Int J Pharmaceutics Drug Anal 4(5):227–233
32. Akbarzadeh A, Mikaeili H, Zarghami N, Mohammad R, Barkhordari A, Davaran S (2012) Preparation and in vitro evaluation of doxorubicin-loaded Fe_3O_4 magnetic nanoparticles modified with biocompatible copolymers. Int J Nanomedicine 7:511–526. https://doi.org/10.2147/IJN.S24326
33. Shanmugavel S, Karthikeyan V (2014) Synthesis and characterization of layer by layer magnetic nanoparticles of methotrexate and melphalan. World J Pharm Pharmaceut Sci 3:1809–1824
34. Zhang P, Liao L, Zhu G (2019) Performance of PATC-PDMDAAC composite coagulants in low-temperature and low-turbidity. Water Treatment 12:2824. https://doi.org/10.3390/ma12172824
35. Falahati F, Baghdadi M, Aminzadeh B (2018) Treatment of dairy wastewater by graphene oxide nanoadsorbent and sludge separation, using in situ sludge magnetic impregnation (ISSMI). Pollution 4(1):29–41. https://doi.org/10.22059/poll.2017.233196.276
36. Nassar NN (2010) Kinetics, mechanistic, equilibrium, and thermodynamic studies on the adsorption of acid red dye from wastewater by γ-Fe_2O_3 nanoadsorbents. Sep Sci Technol 45(8):1092–1103. https://doi.org/10.1080/01496391003696921